22.3: High Efficiency Electrophosphorescent Organic Light Emitting Diodes using Semitransparent Ag as Anode

H. J. Peng, X. L. Zhu, J. X. Sun, X. M. Yu, M. Wong and H. S. Kwok
Center for Display Research, Department of Electrical and Electronic Engineering
Hong Kong University of Science and Technology, Clear Water Bay, Hong Kong

Abstract

We have significantly improved the emission efficiency in an organic light emitting diode (OLEDs) based on tris(phenyl pyridine)iridium [Ir(ppy)3]. Using a semitransparent Ag with surface modification as anode to replace conventional ITO, excellent light outcoupling and hole injection properties have been realized. The Ag based OLED exhibits a maximum current efficiency of 81 cd/A and power efficiency of 79 lm/W, compared with 46 cd/A and 39 lm/W for an ITO anode device. The improvement is due to a carefully designed microcavity.

1. Introduction

Organic light emitting diodes (OLEDs) using phosphorescent emitters have attracted intensive attention due to the highly efficient emission compared to conventional fluorescent OLEDs. Through harvesting both singlet and triplet excitons, the internal emission quantum efficiency of OLEDs doped with phosphorescent emitters can reach nearly 100% [1,2], corresponding to an external quantum efficiency of around 20%, limited only by the light outcoupling efficiency.

There are several methods reported to improve the coupling efficiency of OLEDs, such as microcavity, mirolens array, low index substrate, nanopatterned photonic crystals etc [3-7]. The microcavity structure has been mostly studied because of its compatibility with conventional thin film deposition technologies. A microcavity OLED usually consists of an asymmetrical structure with organic layers sandwiched between a highly reflective metallic mirror and ITO coated distributed Bragg reflector (DBR) [3,4]. However, the multilayer dielectric thin film structure of the DBR makes the fabrication process complicated.

Semitransparent metal reflectors have also been used in top emitting OLEDs as the top cathode. These top emitting devices also demonstrated higher coupling efficiency than an equivalent bottom-emitting nonmicrocavity device due to a strong microcavity effect [8-10]. Using a similar argument, a bottom emitting device using a single layer of semitransparent metal as the reflector, in this case, as the anode, is expected to have an enhanced coupling efficiency compared with the conventional device using ITO as the electrode.

In this paper, we demonstrate a bottom emitting microcavity OLED employing a semitransparent Ag film as the anode and opaque Al as the cathode (Fig. 1). Using a phosphorescent material, $Ir(ppy)_3$, the Ag anode devices exhibit a maximum efficiency of 81 cd/A and a power efficiency of 79 lm/W. This is much better than the results of 46 cd/A and 39 lm/W for a ITO anode device. The improved efficiencies are attributed to the enhanced hole injection and higher outcoupling efficiency in the microcavity devices.

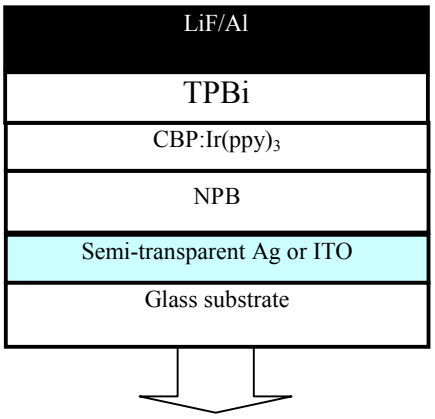

Figure 1. Schematic structure of bottom emitting phosphorescent organic light emitting devices using Ag or ITO as anode.

2. Simulation of microcavity OLEDs using metallic mirrors

In a microcavity OLED, spontaneous emission occurs through radiative exciton decay in a Fabry-Perot (FP) resonator, in which interference effects alter the internal angular power distribution. With an appropriate cavity design, some photons can be moved from the total internal reflection regime to the extraction cone, enhancing the coupling efficiency. Meanwhile, the spontaneous emission rate can be enhanced due to Purcell effect. Therefore, a microcaivty OLED should emit more light than a noncavity one.

The optics of a microcavity OLED can be analyzed by a classical model based on the equivalence between the emission of a photon due to an exciton's radiative decay and the radiation of a classical electrical dipole [11]. In this approach, the power generated $\overline{P}$ by a dipole source can be expressed as an integral over the magnitude of the in-plane wavevector $k_{//}$ that varies from zero to infinite,

$$\overline{P} == \int_0^\infty K(k_{//})dk_{//} \qquad (1)$$

where the quantity $K(k_{//})$ is defined as the $k_{//}$-space power spectrum. Different regions of this $k_{//}$ integration can be identified with different power dissipation channels.

We show in Fig. 2 the calculated $k_{//}$-space power spectra for the cases of an oscillating dipole embedded in a convention ITO anode OLED device and a microcaivty OLED using semi-transparent Ag as anode. The spectra can be divided into four regions according to the $k_{//}$ value:

 ISSN/0005-0966X/05/3602-1066-$1.00+.00

(I)	$0 \le k_{//} \le k_0 = 2\pi/\lambda_0$	Photon emission mode
(II)	$k_0 \le k_{//} \le 1.5k_0$	waveguide mode in glass
(III)	$1.5k_0 \le k_{//} \le 1.7k_0$	waveguide mode in organic layer
(IV)	$1.7k_0 \le k_{//}$	surface plasmon modes.

Here λ_0 is the peak wavelength of photoluminescence spectrum of emitting material which is 516nm for $Ir(ppy)_3$, and k_0 is the corresponding wavevector.

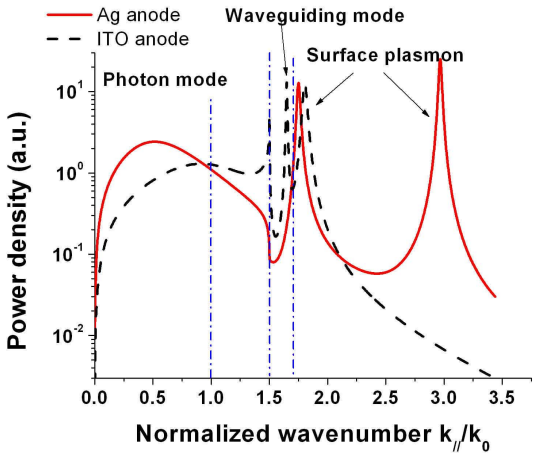

Figure 2. the $k_{//}$-space spectra at a dipole embedded in a bottom emitting OLED with ITO (dashed line) or semitransparent Ag (solid line) as anode.

Region I in the power spectrum corresponds to the photon emission mode, i.e. it gives the portion of the total light that can be extracted from the device surface. Region II and III correspond to waveguiding loss in the glass substrate and the organic layers, respectively. Narrow peaks in region IV are the surface plasmon modes, corresponding to evanescent surface waves propagating along the metallic electrode surface. It can be seen from Fig. 2 that for the Ag anode structure, the power density of the photon mode (Region I) is much larger than that of convention ITO anode structure. At the same time, the waveguide modes in both glass and organic layers are suppressed. As a consequence, the light coupling efficiency of a bottom emitting OLED employing semitransparent Ag anode can be enhanced by using the microcavity effect.

3. Experiment

Two bottom emitting OLEDs with different anodes were fabricated (Fig. 1). For the ITO anode device, 750 Å thick ITO film was deposited by RF sputtering on glass. For the Ag anode device, 250 Å thick Ag film was deposited by thermal evaporation on glass substrates. In both devices, we used 4,4'-bis(1-napthyl-N-phenyl-amino)- biphenyl (NPB) as the hole transport layer, 4,4'-*N*,*N*'-dicarbazole-biphenyl (CBP) doped with fac tris (2-phenylpyridine) iridium (Ir(ppy)3) as the emitter layer, 1,3,5-Tris (N-phenylbenzimidazol-2-yl)benzene (TPBi) as the electron injection layer[12], and LiF/Al as the composite cathode.

For the ITO anode device, the structure consists of

ITO/NPB(70nm)/CBP:$Ir(ppy)_3$(x%)(30nm)/TPBi(40nm)/LiF(1nm)/Al(110nm)

For the Ag anode device, the structure consists of

Ag/NPB(52nm)/CBP:$Ir(ppy)_3$(18nm)/TPBi(40nm)/LiF(1nm)/Al(110nm).

One challenge to using Ag as the anode is its relatively low work function, which leads to a barrier for holes injected to the organic layer. In order to enhance the hole injection ability, the Ag anode surface was modified before the organic film deposition by a novel method developed by our group [13].

All the materials in the devices, including the semitransparent Ag anode were deposited by thermal evaporation in a multi-chamber vacuum system without breaking the vacuum. The base pressure of the system was $<1x10^{-4}$ Pa. In order to avoid cross contamination, the organic materials and the metals were deposited in two independent chambers separated by a gate valve.

Current density(J) - Voltage (V) - Luminance (L) characteristics and were measured using an HP4145B semiconductor parameter analyzer and a large diameter (2.5cm) photodiode. The quantum efficiencies of the devices were measured directly by placing the device about 2 mm over the photodiode. The spectral characterization and the luminance calibration of the photodiode were performed with a PhotoResearch PR650 spectroradiometer.

4. Results and discussion

Figure 3 shows the dependence of external quantum efficiency (η_{QE}) of the ITO anode devices on the $Ir(ppy)_3$ doping concentration in CBP. With the $Ir(ppy)_3$ concentration varying from 2% to 10%, the η_{QE} increases first, achieving a peak value of 12.5% at dopant concentration of 8%, and then decreases. The inset in Fig. 2 shows the corresponding emission spectrum of the devices with various $Ir(ppy)_3$ doping concentration. At concentrations higher than 6%, we only observe the electroluminescence (EL) spectrum peaked at 516 nm due to the $Ir(ppy)_3$ phosphorescence. At concentrations below 4%, an additional blue emission due to NPB fluorescence also appears, which dramatically reduce the device quantum efficiency. The drop of the η_{QE} beyond the optimized concentration is attributed to the aggregate quenching [14].

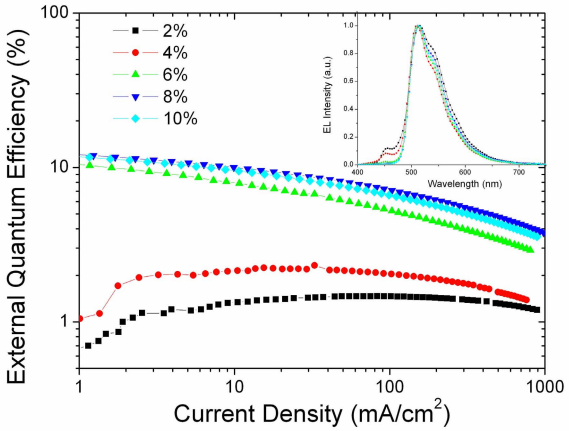

Figure 3. η_{QE} of the ITO anode devices with various $Ir(ppy)_3$ doping concentration.

Fig. 4 compares the current density (J) - luminance (L) –

voltage (V) of the ITO anode device and Ag anode device. Both anodes were pretreated prior to the deposition of the organic layers. The doping concentration of $Ir(ppy)_3$ is 8% for both devices. The Ag anode device shows a performance superior to that of the ITO anode device in both the J-V and L-V curves. For instance, the driving voltages at a current density of 100 mA/cm^2 for devices with the Ag and ITO anode are 7.8 and 10.3 V, respectively. And the voltages to obtain a luminance of 1000 cd/m^2 for the two devices are 4.5 and 6.3 V, respectively. With increasing voltage, both the current density and luminance of the pretreated Ag anode device increase faster than those of the ITO anode device.

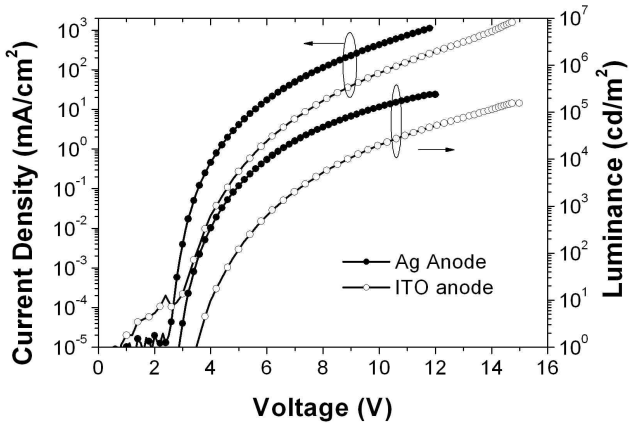

Figure 4. J-V-L characteristics of Ag anode and ITO anode phosphorescent OLED.

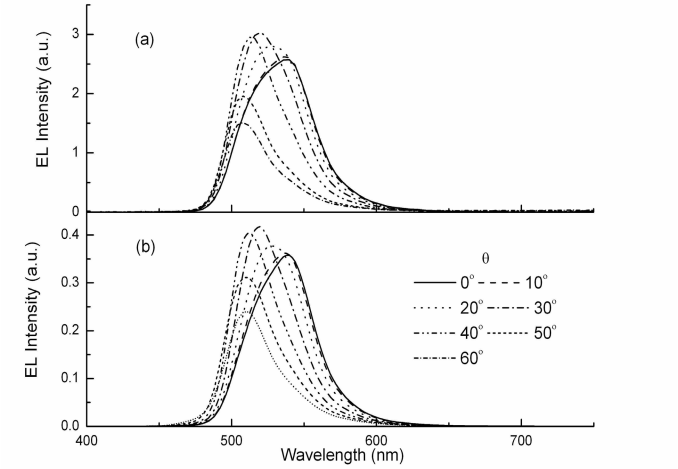

Figure 5. The measured (a) and simulated (b) EL spectra of the Ag anode devices for viewing angles from 0° to 60°.

Bottom emitting devices with reflecting anodes and cathodes are expected to exhibit strong micro-cavity effects on both the spectral and spatial distribution of the emission. Fig. 5(a) shows the EL measured spectra under a current of 2 mA/cm^2 at viewing angles from 0° to 60° from the normal direction for the Ag anode. When the viewing angle increases, the emission peak shifts from 536nm to 516 nm. The emission spectra are also simulated using an optical model based on classical electrodynamics theory. The simulation results are given in Fig. 5(b). It can be seen that the calculated spectra agree quite well with the experimental data.

Fig. 6 shows the power efficiency (η_P) and the current efficiency (η_J) of both devices. The maximum η_J and η_P of the Ag anode device are 81 cd/A and 79 lm/W, respectively, compared with those of 46 cd/A and 39 lm/W for the ITO anode device. At the luminance of 1000 cd/m^2, the Ag anode device still demonstrates a high power efficiency of 47 lm/W, compared with that of 19 lm/W for the ITO anode device. The key values of the two devices are listed in Table 1.

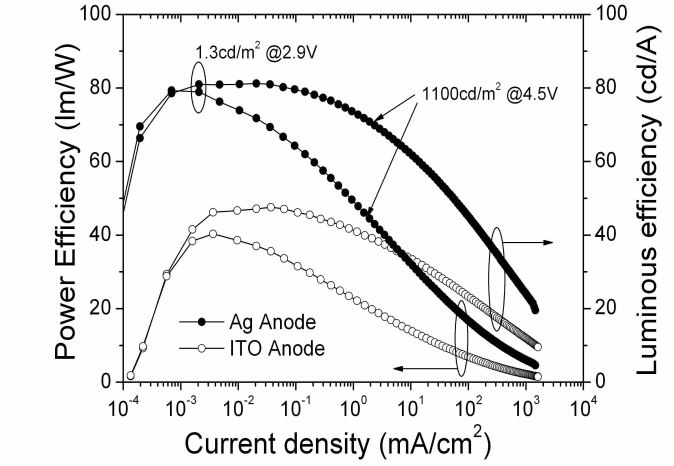

Figure 6. Power efficiency (η_P) and the current efficiency (η_J) of both devices of the Ag anode and ITO anode device

Table 1. Comparison of the EL performance of bottom emitting phosphorescent devices using ITO anode and semitransparent Ag anode.

	Voltage @ 1 cd/m^2	Voltage @ 100 cd/m^2	η_J @ 1mA/cm^2	η_{QE} @ 1mA/cm^2
ITO anode	3.45 V	4.9V	41. 4 cd/A	11.3%
Ag anode	2.75 V	3.65V	72. 7 cd/A	17.5%

The superior performance of the Ag anode device are attributed to the enhanced hole injection ability and the enhanced outcoupling efficiency in the microcaivty structure. It is noticed that the enhancement factor of the power efficiency (η_P) is larger than that of the current efficiency (η_J). The reason is that the enhanced hole injection causes the lower driving voltage of the Ag anode device which consumes less electrical power to obtain the identical current density. The mechanism for the hole injection enhancement of Ag anode will be discussed elsewhere [13]. The improvement of η_J is mostly attributed to the enhanced coupling efficiency. Theoretical simulation predicts that the coupling efficiency can be further enhanced from the Ag anode device with appropriate layer thickness design. However there is stronger color shift effect as well. One should therefore balance the need

for high efficiency and emitting color variation in the microcavity device.

5. Summary

In conclusion, we have demonstrated a high efficiency electrophorphorescent OLED using semitransparent Ag as the anode. The microcavity structure formed by the semitransparent anode and reflective cathode can effectively enhance the outcoupling efficiency of the device. Moreover, with proper surface modification, the hole injection ability of the anode can be enhanced significantly as well. The results show that the maximum η_J and η_P of the Ag anode device are 81 cd/A and 79 lm/W, respectively, compared with those of 46 cd/A and 39 lm/W for the ITO anode device. We believe that a power efficiency over 100 lm/W can be achieved by combining this microcavity structure and the high efficient phosphorescent emitting system [1,2].

Acknowledgements

This work was supported by the Research Grants Council of the Hong Kong Special Administrative Region

References

[1] C. Adachi, M. A. Baldo, M. E. Thompson, S. R. Forrest, J. Appl. Phys.,**90**, 5048 (2001).

[2] M. Ikai, S. Tokito, Y. Sakamoto, T. Suzuki, and Y. Taga, Appl. Phys. Lett. **79**, 156 (2001).

[3] R.H. Jordan, L. J. Rothberg, A. Dodabalapur, and R. E. Slusher, Appl. Phys. Lett., **69**, 1997 (1996).

[4] H. J. Peng, M. Wong, and H. S. Kwok, SID03 Digest, p516 (2003).

[5] S. Möller and S. R. Forrest, J. Appl. Phys. **91**, 3324 (2002).

[6] T. Tsutsui, M. Yahiro, H. Yokogawa, K. Kawano, M. Yokoyama, Adv. Mater., **13**, 1149 (2001).

[7] Y.J. Lee, S. H. Kim, J. Huh, G. H. Kim, Y. H. Lee, S. H. Cho, Y. C. Kim, and Y. R. Do, Appl. Phys. Lett. **82**, 3779 (2003).

[8] M. H. Lu and J. C. Sturm, J. Appl. Phys. **92**. 595 (2002).

[9] C. Qiu, H. J. Peng, Z. L. Xie, H. Y. Chen, M. Wong and H. S. Kwok, SID04 Digest, p (2003).

[10] H. Riel, S. Karg, T. Beierlein, B. Ruhstaller, and W. Riess, Appl. Phys. Lett. **82**, 466 (2003).

[11] W. Lukosz, Phys. Rev. B., **22**, 3030 (1980).

[12] L. S. Liao, K. P. Klubek, and C. W. Tang, Appl. Phys. Lett. **84**, 167 (2003).

[13] H. J. Peng, M. Wong, and H. S. Kwok, unpublished.

[14] S. Lamansky, P. I. Djurovich, F. Abdel-Razzaq, S. Garon, D. L. Murphy, and M. E. Thompson, J. Appl. Phys. **92**, 1570 (2002).